9-12-2023

The role of leading-edge serrations in controlling the flow over owls' wing

Tanner Saussaman
Coastal Carolina University

Asif Nafi
Coastal Carolina University

David Charland
George Washington University

Hadar Ben-Gida
University of Toronto

Roi Gurka
Coastal Carolina University

Bioinspiration & Biomimetics

The role of leading-edge serrations in controlling the flow over owls' wing

IOP Publishing Bioinspir. Biomim. 18 (2023) 066001 https://doi.org/10.1088/1748-3190/acf540

Bioinspiration & Biomimetics

OPEN ACCESS

RECEIVED
6 February 2023

REVISED
14 August 2023

ACCEPTED FOR PUBLICATION
30 August 2023

PUBLISHED
12 September 2023

PAPER

The role of leading-edge serrations in controlling the flow over owls' wing

Tanner Saussaman[1], Asif Nafi[1], David Charland[2], Hadar Ben-Gida[3] and Roi Gurka[1,*]

[1] Physics and Engineering Science, Coastal Carolina University, Conway, SC, United States of America
[2] Mechanical and Aerospace Engineering, George Washington University, Washington, DC, United States of America
[3] Institute for Aerospace Studies, University of Toronto, Toronto, ON, Canada
[*] Author to whom any correspondence should be addressed.

E-mail: rgurka@coastal.edu

Keywords: owl, leading-edge serrations, angle of attack, turbulence suppression

Supplementary material for this article is available online

Abstract

We studied the effects of leading-edge serrations on the flow dynamics developed over an owl wing model. Owls are predatory birds. Most owl species are nocturnal, with some active during the day. The nocturnal ones feature stealth capabilities that are partially attributed to their wing microfeatures. One of these microfeatures is small rigid combs (i.e. serrations) aligned at an angle with respect to the incoming flow located at the wings' leading-edge region of the primaries. These serrations are essentially passive flow control devices that enhance some of the owls' flight characteristics, such as aeroacoustics and, potentially, aerodynamics. We performed a comparative study between serrated and non-serrated owl wing models and investigated how the boundary layer over these wings changes in the presence of serrations over a range of angles of attack. Using particle image velocimetry, we measured the mean and turbulent flow characteristics and analyzed the flow patterns within the boundary layer region. Our experimental study suggests that leading-edge serrations modify the boundary layer over the wing at all angles of attack, but not in a similar manner. At low angles of attack ($<20°$), the serrations amplified the turbulence activity over the wing planform without causing any significant change in the mean flow. At 20° angle of attack, the serrations act to suppress existing turbulence conditions, presumably by causing an earlier separation closer to the leading-edge region, thus enabling the flow to reattach prior to shedding downstream into the wake. Following the pressure Hessian equation, turbulence suppression reduces the pressure fluctuations gradients. This reduction over the wing would weaken, to some extent, the scattering of aerodynamic noise in the near wake region.

1. Introduction

The flight of a bird is characterized by its aerodynamic properties. The boundary layer formed over the wing surface determines its flight performance, which may vary depending on its flight mode. Avian flight comprises various modes, such as gliding, flapping, soaring, and intermittent, depending on the goal of migration, hunting, etc. The simplest form of avian flight is gliding. Birds utilize gliding to save energy; during this phase, they adjust and fix the wing's shape based on the flow conditions to optimize the flight's power cost (Cheney *et al* 2021). In steady gliding flight, the airflow pattern over the wings of a bird can be similar to that of low-to-moderate Reynolds number airfoils (Withers 1981, Lian and Shyy 2007, Winslow *et al* 2018, Anyoji and Hamada 2019). In this low-to-moderate Reynolds number flow regime, complex viscous flow phenomena, such as transition, recirculation, and laminar separation bubble (LSB) (Ellsworth and Mueller 1991, Lian and Shyy 2007) formation, are normally prevalent within the boundary layer of the wing/airfoil. Interestingly, these flow features are also present in bird-like airfoils (highly cambered) at low-to-moderate Reynolds number regimes (Ananda and Selig 2018). However,

many avian species are also known to be highly efficient in terms of aerodynamic performance, implying that their wings can mitigate these flow features that are highly detrimental to flight performance. Indeed, many birds are equipped with some unique morphological features that play important roles in enhancing their aerodynamic performances, like the alula, which is known to increase lift and delay stall during slow flights at high angles of attack (Lee *et al* 2015), wing sweep for sustained flights (Liechti *et al* 2013), long primary feathers to create 'slots' that help with soaring (Klaassen van Oorschot *et al* 2017), etc.

The study presented here focuses on the aerodynamics of owl wings. Owls are slow-flying, non-migratory raptors that are well known for their silent flight capabilities (Wagner *et al* 2017). Most clade members produce sound frequencies that are inaudible to humans and, more importantly, to most of their prey (Neuhaus *et al* 1973, Bachmann *et al* 2007, Sarradj *et al* 2011). Graham (1934) suggested that owls' silent flight capability stems from their wings' special characteristics. He identified three unique wing microfeatures that jointly appear in most owl species: (i) leading-edge serrations, (ii) trailing-edge porous fringes, and (iii) porous, velvety, down feathers distributed over the upper wing surface, as shown in figure 1 (left). All three of these features have been noted over the years to play a role in aerodynamics and aeroacoustics during flight (i.e. Klän *et al* 2012, Wagner *et al* 2017), coupled with the wing's flexibility (i.e. Winzen *et al* 2016) and are summarized at large in Wagner *et al* (2017) and later on in Jaworski and Peake (2020).

The wing microfeature that encounters the flow field first is the leading-edge serrations which were suggested to be responsible for reducing vortex-interaction noise originating from the wing leading-edge interacting with a 'turbulent air stream' (Graham 1934) or quasi-turbulent (Lilley 1998). These leading-edge serrations on owl wings are static hook-like connected and aligned at an angle with respect to the leading-edge surface located at their 10th primary feathers with a size of $\approx$2 mm (Bachmann *et al* 2007). Owls' flights fall within the intermediate ($\sim$50 000 to $\sim$100 000) Reynolds number range (Wagner *et al* 2017). In this region, where both the inertial and the viscous forces cannot be ignored, the flow is assumed to be turbulent. Thus, we postulate that the serrations may alter the turbulent boundary layer over the wing, impacting the near wake flow characteristics and, potentially, the aerodynamic performance, as suggested by Ito (2009).

Kroeger *et al* (1972) and Anderson (1973) investigated the aerodynamic functions of leading-edge serrations. They suggested that these serrations are responsible for turning the flow close to the leading-edge in the spanwise direction (toward the wingtip), hypothesizing that they generate a stationary leading-edge vortex (LEV) that delays flow separation and produces nonlinear lift on the outer half of the owl wing (common over delta wings (Lowson and Riley 1995)). Geyer *et al* (2017), through flow visualization, found similar trends in the flow over the wing. The formation of a stationary LEV, as found in low-aspect-ratio delta wings at relatively high angles of attack (Gursul *et al* 2007, Linehan and Mohseni 2020) and more recently on high-aspect-ratio swept wings (Ben-Gida and Gurka 2022), can yield a significant nonlinear lift enhancement.

Over the years, few studies have been published on boundary layer formation over prepared or stuffed owl wings in wind tunnel experiments. Klän *et al* (2009) demonstrated that a separation bubble caused by an adverse pressure gradient occurs at approximately 20% of the chord length of a barn-owl wing. It has been suggested that leading-edge serrations (Schwind and Allen 1973, Klän *et al* 2010) and velvety down feathers (i.e. Klän *et al* 2012, Winzen *et al* 2012a, 2012b, 2013) suppress the separation bubble by shifting the detachment point back and reattachment point forward. High-resolution particle image velocimetry (PIV) studies were conducted by Winzen *et al* (2014) using a straight artificial serration placed at the leading edge of a wing model (designed using an owl-based airfoil). They observed that the size of the LSB (Ellsworth and Mueller 1991, Lian and Shyy 2007) generated by rigid artificial serrations was almost independent of the Reynolds number. The integral length scale was also estimated for different angles of attack and Reynolds numbers. They concluded that the upper surface of a clean wing had smaller vortices than one with serrations. Rao *et al* (2017) conducted a combined study of numerical and experimental measurements on a single-feather-wing model. They showed that leading-edge serrations could control the laminar-to-turbulent transition on the suction side of the model for all angle of attack (AoAs). Furthermore, they showed that noise is suppressed across all angles whilst the aerodynamic performances behaved in opposed manner depending on the AoA: $<15°$; reduction and $>15°$; enhancement. Lawley *et al* (2019) showed using long-duration high-speed PIV that the downstream wake flow of a freely flying boobook owl is composed of flow scales that are an order of magnitude smaller than non-owl species (European starling and Western sandpiper), and the turbulence dissipation in this region was significantly high. However, the underlying mechanisms associated with the suction boundary layer dynamics have yet to be characterized in the presence of micro-structure serrations at the leading-edge region. Furthermore, it is unclear how these serrations impact the turbulent field over the wing for a range of angles of attack.

In essence, the flow pattern over bird airfoils resembles that of a low to intermediate Reynolds number airfoil, but the inclusion of microfeatures significantly changes the flow properties/scales. The presence of leading-edge serrations in most owl species suggests they play a unique role during flight; however, the underlying mechanisms associated with turbulence remain unclear. Inspired by this feature, we present a comparative study between two owl-based wing models with and without leading-edge serrations. This experimental study aimed to characterize how the boundary layer developed over the upper surface of the wing is affected by the presence of serrations. We used the geometrical parameters of leading-edge serrations of a barred owl. It is acknowledged that these parameters vary across different owl species (Weger and Wagner 2016), yet the morphological patterns are similar. This paper comprises the experimental details, followed by a discussion of the results, and concludes with a summary of the findings.

2. Methods

To analyze the effects of leading-edge serrations on the flow dynamics around the owl wing, a controlled study using two wing models (with and without serrations) in a recirculating water flume was performed. Optical flow measurement techniques were used to measure the flow within the boundary layer that developed over the wing.

2.1. Owl wing model

A dead barred owl wing was electronically scanned, as shown in figure 1(A), and was used to generate a 3D model in SolidWorks (see figure 1(B)). This model was 3D printed into two configurations: (i) a baseline wing with a smooth leading edge and (ii) with leading-edge serrations. This enables a comparative evaluation of the effect of leading-edge serrations on the flow over the wing. The printed wing models were 1:2 of the full scale to fit within the flume and avoid blockage effects (the blockage ratio was $<$2.5%). Both wings have a span of 0.21 m and an average chord length (C) of 0.11 m. The leading-edge features were re-scanned to generate a more accurate replica of the serrations, given their small size. The scanned serrations were then imported into a digital model. The serrations were 3D printed separately and glued back to the wing at the leading edge to reduce the possibility of errors during 3D printing. The geometry of the printed serrations was based on averaging the geometrical dimensions of the serrations along the span. The variation in serrations along the span was relatively low ($\pm$0.5 mm). The serrations were attached to the center of the leading-edge region. The leading-edge serrations were each 2 mm (0.018% of the chord length) in length with a diameter of 1 mm, attached at an angle of 110° normal to the leading-edge surface.

The experiments investigated the downstream flow dynamics and suction surface boundary layer characteristics as functions of AoA. The PIV technique was used to measure the boundary layer region over the upper surface with a high spatial resolution.

3. Experimental setup

The two wing models were tested using a recirculating water flume. The water flume is composed of a 15 m long open channel with a cross-section of 0.5 m by 0.7 m, where the middle 5 m is made of tempered glass, as shown in figure 2: left. Two large holding reservoirs exist at either end of the channel. The water depth in the channel was maintained constant at 0.36 m. A large centrifugal pump with a flow rate capacity of up to 3028 LPM (800 GPM) was used to generate the flow. The pump rotation speed was controlled using a variable frequency drive. The uniform flow velocity within the channel was estimated as $U = Q/A = 0.19$ ms^{-1}, where Q is the flow rate measured by a rotary flow meter, and A is the cross-sectional area of the water in the flume. The flow velocity yields a chord-based Reynolds number of $Re_c = UC/\nu = 49\,000$ for all experiments, where C is the root chord length (0.11 m) and ν is the kinematic viscosity of water ($1.11{\cdot}10^{-6}$ m^2 s^{-1} at 22 °C).

2D-PIV was utilized to obtain measurements in the streamwise and wall-normal planes. The wings were mounted upside down so that the flow over the top of the wing could be measured when illuminated by a light sheet emanating underneath the flume, as shown in figure 2 (right). The mount consisted of an elongated bar placed on the flume sidebars, where a thin elongated rod was connected between the bar and wing. The rod diameter was less than 1 cm to minimize disturbances to the incoming flow. The experimental setup is shown in figure 2. A dual-pulsed Nd:YAG laser (Quantel, Inc. EverGreen 145) operating at 145 mJ per pulse and a wavelength of 532 nm was used to illuminate the flow with a light sheet approximately 1 mm thick. The particles used in the flume were fused borosilicate glass microspheres with an average diameter of 11 μm (Potters Industries). PIV images were captured with a 29MP double exposure CCD camera (PowerView^{TM}) with a dynamic range of 12 bits operating at 1 Hz with a Nikon 105 mm lens. This setup resulted in velocity field images of 0.31 m $\times$ 0.21 m.

Five hundred image pairs were collected for each experiment and analyzed using cross-correlation (Insight 4G, TSI Inc.) to estimate the two velocity components in the streamwise (u) and wall-normal (v) directions over the (x, y) plane. Each image pair was divided into interrogation regions of 64 $\times$ 64 pixels with 50% overlap for cross-correlation,

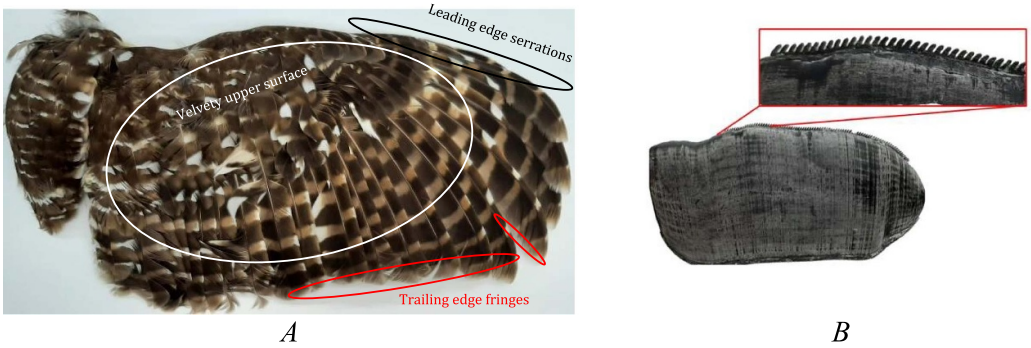

Figure 1. (A) Barred owl wing (left) with the specific features commonly found in nocturnal owls' species: leading-edge serrations, velvety upper surface (elongated pennula), and trailing-edge fringes. (B) 3D printed wing with a closeup of the serrations.

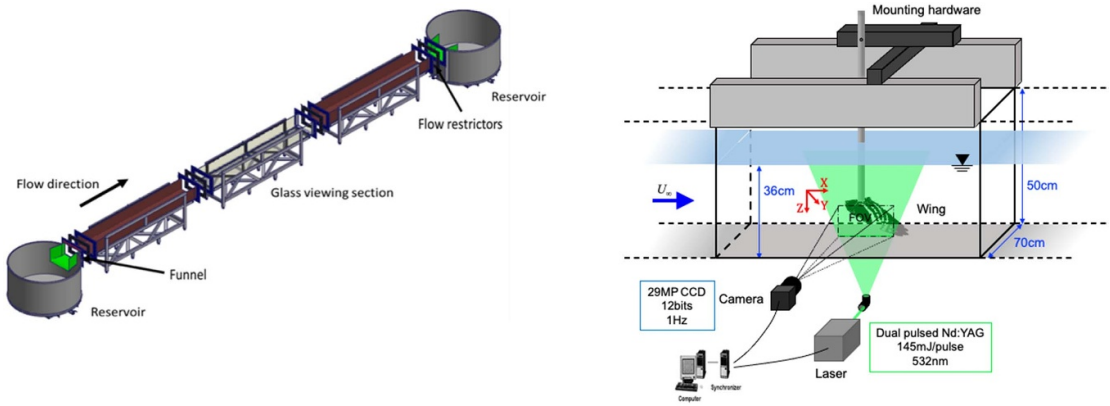

Figure 2. Schematic illustration of the experimental setup. Left: the recirculating water flume. Right: the mounting system of the owl wing and the PIV system, including the laser, camera, synchronizer–computer system, and field of view captured by the PIV.

yielding 500 vector maps per experiment to allow for statistical convergence. The vector maps were subsequently filtered for outliers by using local and global filters. The uncertainty in the instantaneous velocities was estimated to be approximately 2%–4% of the measured value, while the computed instantaneous velocity gradients had an uncertainty of 8%–10% (Huang *et al* 1997, Raffel *et al* 2007). Bootstrap error estimates for the mean and root-mean-square quantities were computed (Efron and Gong 1983). The nominal values are 1.25% for the mean whilst 6%–10% for the multiplications of the velocity fluctuations (i.e.: Reynolds stress) for the smooth and serrated wings, respectively (see appendix A1).

Using this configuration, both 3D printed wings were tested at different angles of attack, $\alpha = 6°$, 12°, and 20°. These angles were set using a digital level ($\pm 0.1°$) and re-measured after each trial. This was performed to ensure that the wing pitch did not change during the test and to avoid any unknown sources of error affecting the results. For each angle of attack, the flow over the wings was measured at five different planes: 0%, 25%, 50%, 75%, and 95% of the wingspan from the root (herein as the root (P1), root-to-mid (P2), mid (P3), mid-to-tip (P4) and tip (P5), respectively) as shown in figure 3: right. Sampling over the wingspan provided a three-dimensional (3D) view of the flow evolution in the spanwise direction.

4. Results

The results section comprises two main subsections: the mean profiles and turbulence characteristics. We present our results in a comparative fashion between the baseline (smooth leading edge) and the serrated wing. The results demonstrate how various flow quantities vary in the spanwise direction as a function of AoA. Most quantities presented herein were averaged over the PIV domain, where their maximum values demonstrated discrepancies between the models (if they existed).

4.1. Boundary-layer characteristics

Given the intermediate Reynolds number, the flow over the wing appears to be turbulent across the span (Coles 1956) (see appendix A2, figures 1 and 2 demonstrating the turbulent nature of the boundary layer). It is noteworthy that the tested model had a smooth surface, and owl wings in nature consisted of a rough velvety surface, suggesting that the flow over the owl wing is mostly turbulent (Klän *et al* 2010, Winzen *et al* 2013).

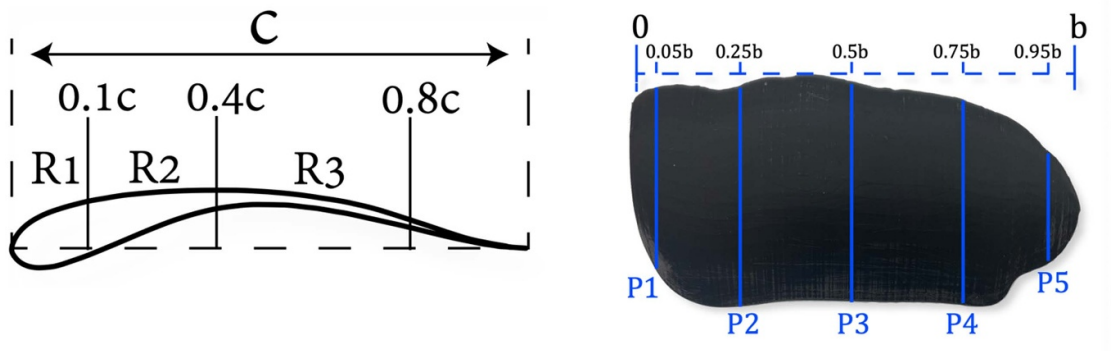

Figure 3. Schematic description of the field of view locations where measurements were performed. Left: wing cross section divided into three arbitrary regions: leading-edge (R1), separation (R2), and reattachment (R3), where C is the chord. Right: wing planform; blue lines represent the five different measured PIV planes where b is the wing spanwise length.

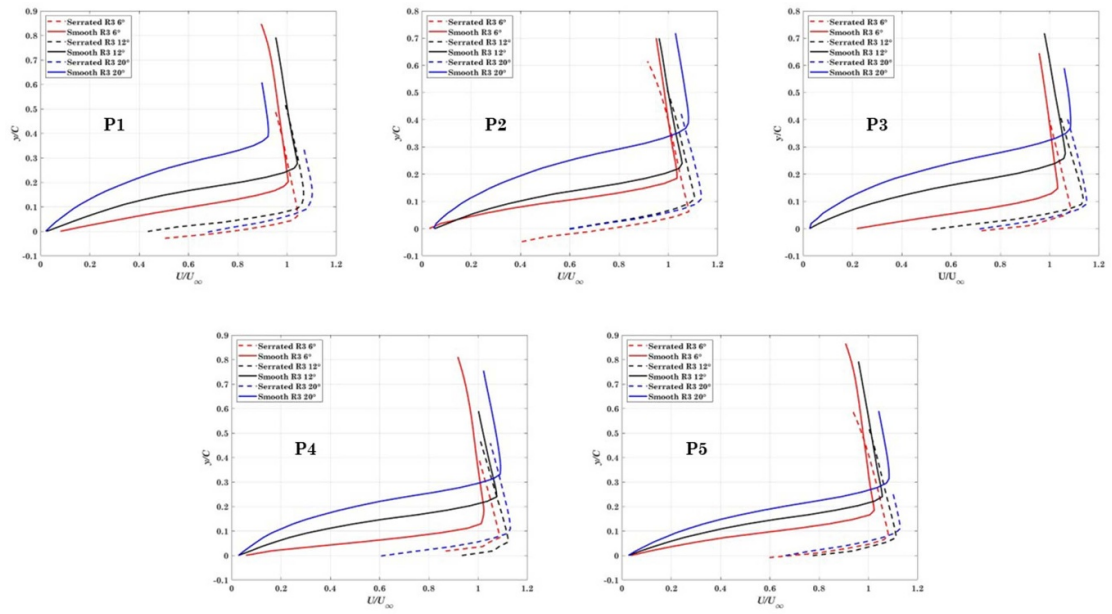

Figure 4. Mean velocity profile normalized by freestream velocity (U_∞) at region R3 for the selected angles of attack at the five measured planes in the spanwise direction. y/C denotes the vertical extent of the PIV window.

To characterize the flow over the wing, we have chosen to qualitatively divide the boundary layer developed over each section of the wing into three regimes (see figure 3: left): (R1) leading-edge: where the boundary-layer is formed (0–0.1C), (R2) separation region: where for relatively high angles of attack, the flow may separate, and the boundary-layer collapses (0.1–0.4C) and (R3) the reattachment region where the flow may re-attach at certain angles of attack and the boundary-layer is reformed (0.4–0.9C). The region close to the trailing edge was not included in the analysis, as laser reflections hitting the edge prevented reliable measurements in this small region.

A sample of the mean velocity profiles for region R3 is shown in figure 4. Mean velocity profiles were calculated for all regions in all planes and AoAs. Regions R1 and R2 showed a marginal difference between the wing models (see appendix A3). However, the velocity profiles at region R3 appear to be different. The smooth wing presents larger velocity gradients than those in the serrated case. A modest slope for the serrated cases suggests that the velocity gradient is smaller; thus, the viscous drag formed over the surface in this region is low compared to the smooth model. For all the planes, the largest gradient obtained was at 20° in R3. The difference in the boundary layer thickness (where y/C corresponds to $U/U_\infty \approx 1$) suggests that the boundary layer experienced a large separation at 20° where the flow was fully separated at this angle (see appendix A2, figure 3). The profile trends for the smooth case over the range of AoA are larger than those of the serrated wing, where the gradient (slope) of the streamwise

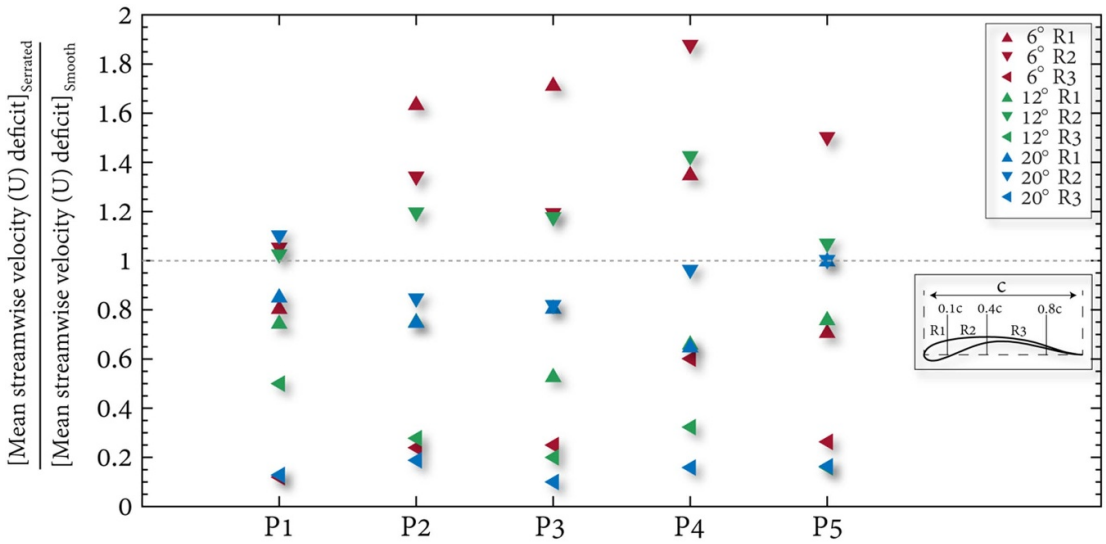

Figure 5. The mean streamwise velocity profile deficit ratio within the boundary layer between the serrated and smooth case in the streamwise-normal planes at different spanwise locations (P1, P2, P3, P4, P5). In the sub-panel, *C* denotes to chord length of the wing.

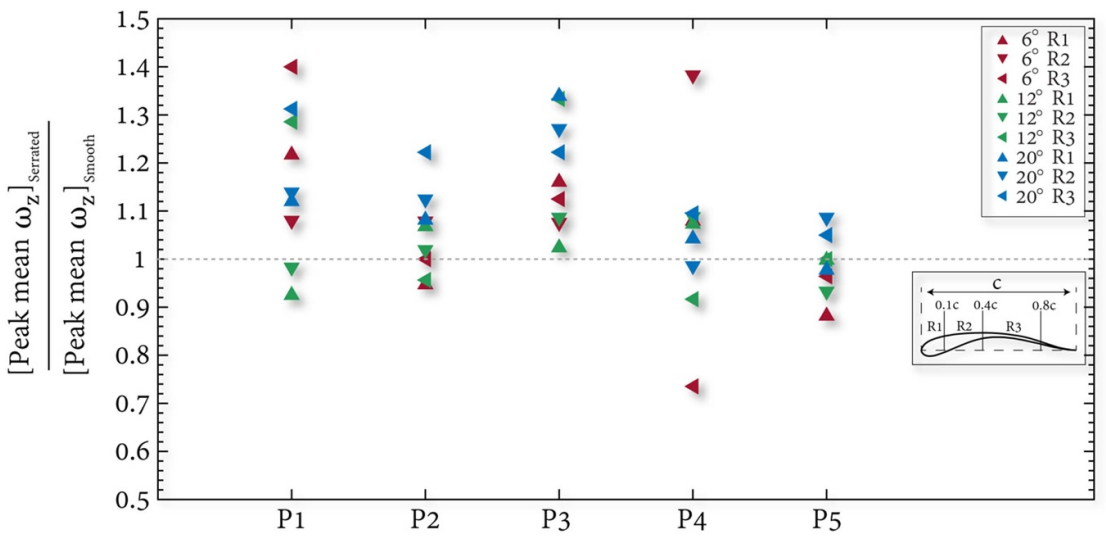

Figure 6. The ratio of the peak mean spanwise vorticity (Ω_z) profile within the boundary layer between the serrated and smooth case in the streamwise-normal planes at different spanwise locations (P1, P2, P3, P4, P5). In the sub-panel, *C* denotes to chord length of the wing.

velocity close to the surface appears to be similar. All the velocity profiles in this region depict an accelerated region due to an adverse pressure gradient occurring at a region of approximately 0.1–0.2*C* over the wing. This acceleration is typical for the region after reattachment over curved surfaces (Sturm *et al* 2012).

Figures 5–8 are comparative ones. For each flow property, the ratio between the serrated and smooth wing was calculated. A value smaller than one indicates that the property value for the serrated case is lower than that for the smooth case, and vice versa if the value is larger than one. Different AoA are colored: 6° red, 12° green, and 20° blue. The three regimes over the wing are depicted as triangular shapes: R1 0°, R2 180° flipped, and R3 90° rotated. The *x*-axis marks the locations over the wingspan: P1 root, P2 between root and mid, P3 mid-section, P4 between mid and tip, and P5 wing tip. For the list of the numbers used to plot these figures, please refer to appendix A5.

Next, the mean velocity profiles were integrated, and the resultant area under the curve was proportional to the displacement deficit (δ) in the boundary layer. Integration was performed on the mean streamwise velocity from the surface up to the region where the velocity value did not change (i.e. the edge of the boundary layer). A smaller area indicates less momentum loss, which may be inferred as

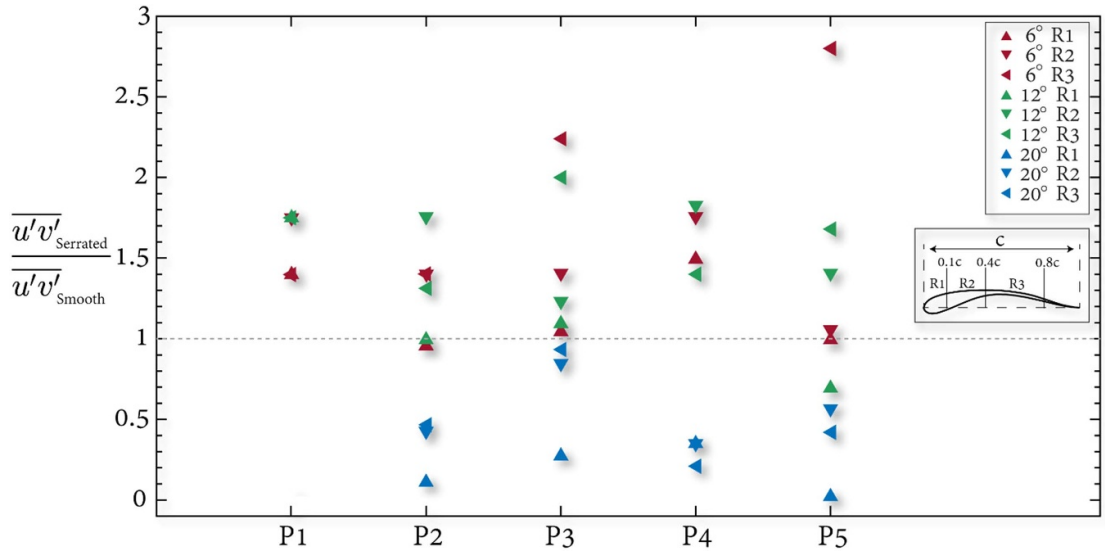

Figure 7. The ratio of the maximal Reynolds stress component ($\overline{u'v'}$) between the serrated and smooth case in the streamwise-normal planes at different spanwise locations (P1, P2, P3, P4, P5). Here, u' refers to streamwise velocity fluctuation, and v' refers to vertical velocity fluctuation.

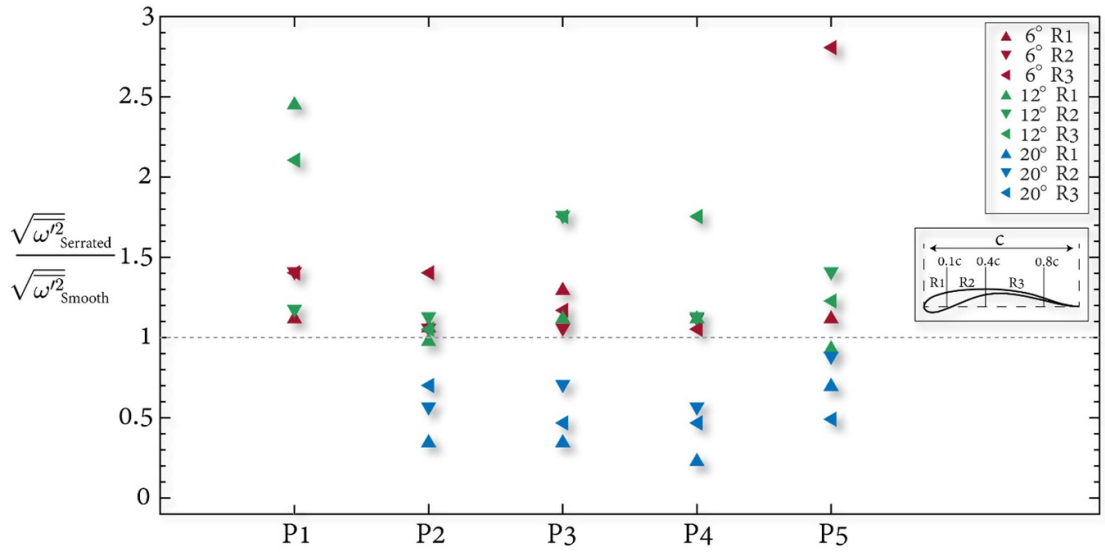

Figure 8. The ratio of the maximal enstrophy ($\sqrt{\overline{\omega'^2}}$) between the serrated and smooth case in the streamwise-normal planes at different spanwise locations (P1, P2, P3, P4, P5). Here, ω' refers to vorticity fluctuation. In the sub-panel, C denotes the wing chord length.

less frictional drag (Schlichting and Kestin 2017). For each region (R1, R2, and R3), this integral was averaged separately for the different AoA. The integral values are presented in figure 5 as the ratio between the serrated and smooth wings. These ratios were calculated over the span (figure 5) and marked as P1, P2, P3, P4, and P5, as described in the experimental setup. At 6°, the presence of leading-edge serrations increases δ compared to the smooth case over the span, at the leading-edge and middle regions. For all AoA across the span, the serrated case at R3, toward the trailing edge, was significantly thinner than the smooth case. For 12° and 20°, this trend also appears at the leading edge but is flipped in the middle section, similarly to the 6° case, demonstrating the dependency of the flow dynamics on AoA (Ben-Gida *et al* 2020).

The differences in the leading edge suggest that the initial boundary layer developed over the wing generated less frictional drag in the presence of serrations at high AoA. Over the last section of the boundary layer, the presence of serrations caused less momentum loss over the surface for all tested cases suggesting that serrations decrease momentum loss on average. The mean spanwise vorticity over the wing was calculated to complement the characterization of the boundary layer. An example of the mean vorticity profiles is presented in appendix A4.

Maximum values obtained for the mean spanwise vorticity were chosen for comparison within the boundary layer. With the assumption that the spanwise vorticity over the boundary layer is a strong function of dU/dy rather than dV/dx (Schlichting and Kestin 2017, p 670), the vorticity profiles obtain a dominant maximum value close to the surface and decays exponentiality far from it. The ratio of these maximal values within the boundary layer between the serrated and smooth wings is shown in figure 6. For 20°, the ratio across the span is greater than 1. For 6° and 12°, mixed values across the span were observed, similar to those in figure 5. Though it seems that, for most points, the ratio is larger than 1. These ratios did not feature any apparent trend to distinguish between the AoA studied over the wingspan.

4.2. Turbulent characteristics over the wing surface

The influence of serrations on the turbulence developed over the wing suction surface has also been examined. It is noteworthy that the AoA and planform geometry are coupled with the presence of serrations, which may cause modulation of turbulence within the boundary layer compared to the smooth leading-edge case. In this study, turbulence modulations were characterized through the distributions of the Reynolds stress and spanwise enstrophy over the wing planform within the boundary layer region. These quantities were calculated from the PIV data over five different spanwise locations at three different AoA, similar to the procedures shown in figures 5 and 6. Similarly, for each region, the maximum value of the turbulent quantity was calculated, and for each of the five planes, three values were obtained for the smooth and serrated wings. The choice of the maximal value was to emphasize the conditional differences between the planes and angles of attack coupled with the presence/absence of serrations at the leading edge. For example, an average value may not be representative because of smearing effects over the region. To compare the effect of turbulence on the presence of serrations, the ratio of turbulent quantities between the serrated and smooth cases was calculated. With this, a value smaller than one may suggest a reduction in the calculated turbulent property when introducing serrations. When the ratio exceeds one, an enhancement is achieved for the same property.

Figure 7 presents the ratios of the maximal Reynolds stress component in the streamwise-normal planes as a function of the AoA and location over the wing planform. The x-axis represents the plane location as detailed in the experimental setup section (P1, P2, P3, P4, and P5), and the y-axis represents the Reynolds stress ratio. The absolute values of the maximal Reynolds stress within the boundary layer show a consistent trend, where the Reynolds stress increases across planes with an increase in the angle of attack. The values at the root location were somewhat inconsistent, as the flow in this region may have been impacted by edge effects, where the rod holding the wing was connected. In general, the ratios at 6° and 12° are higher than 1. The only exceptions were at the leading-edge region in the tip (for 12° R1, shown in figure 7) and P2 (for 6° R1, shown in figure 1). At 20°, the ratio over the wing was lower than one. Values above and below one are sparsely distributed. This distribution suggests that the serrations do not affect the turbulence level linearly because their effect is coupled with the AoA and geometrical planform of the wing (resembling a natural owl wing), which is not symmetrical. Similar trends occur in the turbulent kinetic energy distribution at the boundary layer (see appendix A6: figure 1 for the turbulent kinetic energy ratio), suggesting that turbulence is modulated contrastively at different angles of attack owing to the presence of serrations.

The Reynolds stresses and turbulent kinetic energy terms are velocity characteristics, whereas the enstrophy ($\sqrt{\overline{\omega'^2}}$) represents the velocity gradients (see figure 8). For an incompressible fluid, enstrophy is directly proportional to the energy dissipation by viscosity (Doering and Gibbon 2004).

At 12°, the serrations significantly impact the flow at the end section (R3) of the boundary layer across the span, where the ratio is higher than 1.5. At the leading-edge section (R1), for both 6° and 12°, the ratios were close to constant across the span. At 20°, the ratio varies across the span by approximately 20%, although the presence of serrations consistently reduces the level of enstrophy across the wing planform. The enstrophy ratio is higher downstream of the wing than in the leading-edge region for 6° and 12°. At 20°, the ratio at the leading edge indicates stronger suppression of the enstrophy at the leading edge compared to the downstream, where the bubble and reattachments occur, given that separation over the wing at this AoA occurs.

The notion that serrations at high AoA suppress turbulence is presumably coupled with the boundary layer structure of the flow developed over the wing at 20°. Therefore, the impact of serrations on the flow structures at this AoA was examined. To characterize the boundary layer structure over the wing, a conditional sampling technique known as proper orthogonal decomposition (POD) (Berkooz *et al* 1993, Gurka *et al* 2006, Diamessis *et al* 2010, Taylor *et al* 2013) was utilized. POD was applied to the velocity fields within the boundary layer region only. POD was applied to the PIV data collected at 20° for the two cases in planes P2–P4. The decomposition yielded an energy conversion of the modes where 93%–94% (smooth) and 95%–96% (serrated) of the energy was stored in the first 30 POD modes for the three planes. Figure 9 depicts the energy distribution over the first ten POD modes for the different planes and wing configurations. The energy represents the kinetic energy

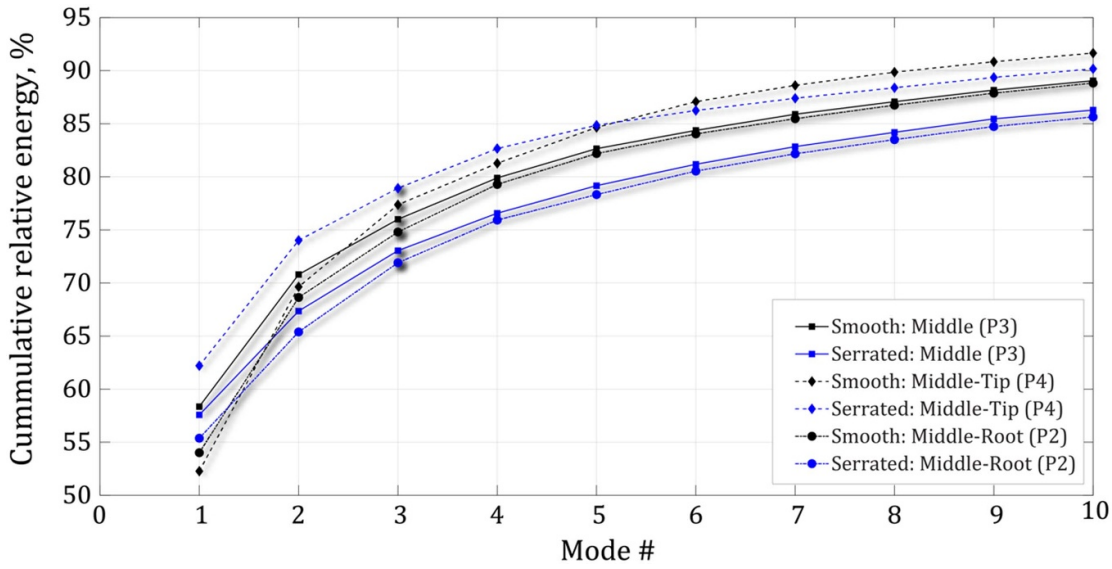

Figure 9. POD modes energetic commutative distribution. Energy distribution over the first ten modes. The data is based on PIV velocity maps acquired at 20° at the P3 plane.

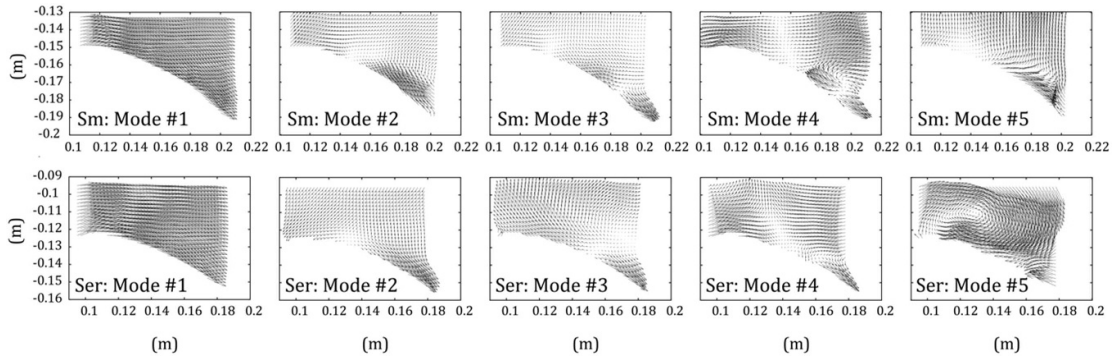

Figure 10. POD modes 1–5 (from left to right) depicted as quiver plots decomposed from the leading-edge region for P4 at 20°. Top: smooth wing ('Sm'); Bottom: serrated wing ('Ser').

of the velocities and spans across the flow scales. The *y*-axis shows the cumulative energy: i.e. for the middle to tip serrated case; the 1st mode contains 62% of the total energy (100%), the 2nd consecutive mode contains 12% (74%–62%), the 3rd mode accounts for 4%, and so on such that the 1st mode is the dominant one representing the mean flow. The subsequent modes, therefore, represent secondary flow events toward turbulent intermediate and small structures (Diamessis *et al* 2010).

One can observe a difference in the energy levels across cases; the flow over the smooth wing contains more energy than the serrated wing across the multiple planes. The general trend indicates that the presence of serrations reduces the kinetic energy level across the turbulence scales. This is in agreement with the results reported here for the Reynolds stress and TKE, showing suppression of turbulence at 20°. A detailed lookup of the first selected modes decomposed from plane P4 is shown in figure 10. A comparison of each mode as a function of wing type shows qualitatively similar patterns over the wing surface. The similarity in patterns suggests that the modulation observed in the turbulence properties is associated mainly with the small flow scales and their overall morphology in this region, as can be seen for modes 4–5 that contain less energy and are presumably associated with small turbulence scales (Taylor *et al* 2013). These qualitative discrepancies indicate that the serrations may act as a passive flow control mechanism to suppress turbulence through the modulation of small scales, that is, by changing the small-scale structures (forming an organized secondary structure), causing a change in the boundary layer formation over the wing, which eventually affects the location of separation and reattachment.

5. Discussion

We describe the impact of leading-edge serrations on the flow dynamics developed over the wing. These serrations are essentially a passive flow control

mechanism used by owls to enhance some of their flight characteristics, as postulated by Kroger *et al* (1972) and later tested by Geyer *et al* (2017), Winzen *et al* (2014) and Winzen *et al* (2015). The main differences between our study and previous ones lie within the serrations' geometry and the detailed observation within the boundary layer over the planform. Numerous studies utilized inspired owls' leading-edge serrations on airfoil to control the aerodynamic noise (i.e. Hersh *et al* 1974, Narayanan *et al* 2015, Hu *et al* 2021) as well as study their impact on aerodynamics (Chaitanya *et al* 2017), yet they used classical airfoils (NACA) as well as relatively simple geometries of the serrations (i.e. sawtooth, wavy, etc). The serrated model used herein was a replica of a scanned barred owl wing matching the geometrical features in terms of shape and positioning angle, unlike the elliptical shapes serrations inspired by owls (Winzen *et al* 2014). In addition, we present a more detailed study of the turbulence dynamics within the boundary layer over the entire planform depicting changes in the spanwise, streamwise, and normal directions for the chosen AoAs. Specifically, characterizing how the small-scales of the flow are impacted by the presence of realistic owl's serrations which have not been addressed to the best of our knowledge.

Our experimental study suggests that leading-edge serrations modify the boundary layer over the wing at all angles of attack, but not in a similar fashion. The boundary layer characteristics over the wing in the static mode (i.e. gliding) result from the wing geometry (planform, thickness, chord length, and sweep angle), AoA, and incoming flow conditions. These parameters determine whether separation and reattachment will occur, the state of the boundary layer (turbulent or laminar), and other phenomena, such as the formation of an LEV. Introducing serrations at the leading edge changes the interaction between wing characteristics and incoming flow conditions. This is a coupled change, that is, the dependency between AoA, planform geometry, and serrations may cause a nonlinear interaction that results in variations in the flow characteristics over the wing as the AoA changes, mainly within the turbulence field. Expected variations were not observed in the mean field characteristics. The mean streamwise velocity and mean spanwise vorticity did not exhibit a clear trend in the difference between the modified and smooth wings. The variations range across the span and angles of attack, indicating that at 20°, because the flow is separated, the serrations reduce the absolute maximal values of spanwise vorticity. In contrast, the trends were inconclusive for the other lower AoAs.

Across all the estimated turbulent characteristics, it was observed that the serrations enhance turbulence at low to moderate AoA. However, at a high AoA, turbulence was suppressed. This suppression is presumably associated with the suppression of the separation bubble causing early reattachment and reducing the turbulence intensity in the upstream flow toward the wake. Winzen *et al* (2014) found a similar reduction in the separation region. They corroborated this finding but noted that the presence of serrations hindered the aerodynamic performances with increasing angle of attack. Nafi *et al* (2020) also showed that the aerodynamic performances of a freely flying owl are low compared with other birds during flapping flight. Similar results were reported by Rao *et al* (2017), who suggested that suppression of turbulence leads to more uniform flow patterns which may lead to noise suppression.

We also observed spanwise variations of the turbulence characteristics for all angles of attack, regardless of enhancement or suppression. However, for 6° and 12°, the variation in the turbulent ratios appears more significant compared with the 20° case. The combination of an elliptical planform shape with a positive angle of attack causes 3D effects on the flow. Unlike delta wings or swept-back wings, where the flow is governed by the presence of coherent patterns (i.e. LEV) developed along the span where one can assume 3D to be quasi-2D, the same cannot be assumed when introducing serrations. However, at higher angles of attack, fewer variations were observed across the span.

Boundary-layer structures were characterized using POD to complement the results. We focused on the boundary layer developed over the wing at $\alpha = 20°$, where we showed that the flow for the smooth case separated over the wing. Apparent discrepancies between the serrated and smooth wings were observed. A comparison between the first modes did not reveal any geometrical differences. However, at higher modes, the geometrical features appeared to be different. Higher POD modes are commonly associated with smaller turbulence scales, suggesting that the serrations manifest the entire turbulent boundary layer field by altering these scales over the surface. Interestingly, the serrations, which are micro-features that should impact the small scale of the flow, locally, manifest the entire boundary layer developed over the wing; thus, a local disturbance generates a non-local impact.

The main question we explored was what causes the turbulence to be suppressed at high angles of attack in the presence of serrations while being enhanced at low angles. From the observed results, it is suggested that at high AoA, the flow that separates over the wing around the leading-edge region does not re-attach and move downstream fully separated. This, in turn, leads to lift reduction and an increase in viscous and profile drag. In the presence of serrations, this separation is suppressed. As a result, the flow reattaches to the wing surface and forms a new boundary layer that is shed into the wake region, presumably causing a lower loss in lift and small profile drag formation (Krishnan *et al* 2020, Nafi *et al* 2020). Furthermore, the separation bubble

is known to increase the airfoil self-noise level (Brooks *et al* 1989), thus, the overall noise. Therefore, by re-attaching the boundary layer, it is plausible to assume that the serrations may also help reduce the broad-band noise.

Data availability statement

All data that support the findings of this study are included within the article (and any supplementary files).

ORCID iDs

Hadar Ben-Gida https://orcid.org/0000-0003-2488-3234
Roi Gurka https://orcid.org/0000-0002-8907-6663

References

Ananda G K and Selig M S 2018 Design of bird-like airfoils *2018 AIAA Aerospace Sciences Meeting*
Anderson G W 1973 An experimental investigation of a high lift device on the owl wing (Air Force Institute of Technology)
Anyoji M and Hamada D 2019 High-performance airfoil with low Reynolds-number dependence on aerodynamic characteristics *Fluid Mech. Res. Int. J.* **3** 76—80
Bachmann T, Klän S, Baumgartner W, Klaas M, Schröder W and Wagner H 2007 Morphometric characterisation of wing feathers of the barn owl *Tyto alba pratincola* and the pigeon *Columba livia Front. Zool.* **4** 1–15
Ben-Gida H and Gurka R 2022 The leading-edge vortex over a swift-like high-aspect-ratio wing with nonlinear swept-back geometry *Bioinsp. Biomim.* **17** 066016
Ben-Gida H, Gurka R and Weihs D 2020 Leading-edge vortex as a high-lift mechanism for large-aspect-ratio wings *AIAA J.* **58** 2806–19
Berkooz G, Holmes P and Lumley J L 1993 The proper orthogonal decomposition in the analysis of turbulent flows *Annu. Rev. Fluid Mech.* **25** 539–75
Brooks T F, Pope D S and Marcolini M A 1989 *Airfoil Self-Noise and Prediction* (NASA Reference Publication) p 1218
Chaitanya P, Joseph P, Narayanan S, Vanderwel C, Turner J, Kim J W and Ganapathisubramani B 2017 Performance and mechanism of sinusoidal leading edge serrations for the reduction of turbulence–aerofoil interaction noise *J. Fluid Mech.* **818** 435–64
Cheney J A, Stevenson J P J, Durston N E, Maeda M, Song J, Megson-Smith D A, Windsor S P, Usherwood J R and Bomphrey R J 2021 Raptor wing morphing with flight speed *J. R. Soc.* **18** 1–14
Coles D 1956 The law of the wake in the turbulent boundary layer *J. Fluid Mech.* **1** 191–226
Diamessis P J, Gurka R and Liberzon A 2010 Spatial characterization of vortical structures and internal waves in a stratified turbulent wake using proper orthogonal decomposition *Phys. Fluids* **22** 086601
Doering C R and Gibbon J D 2004 *Applied Analysis of the Navier-Stokes Equations* (Cambridge University Press)
Efron B and Gong G 1983 A leisurely look at the bootstrap, the jackknife, and cross-validation *Am. Stat.* **37** 36–48
Ellsworth R H and Mueller T J 1991 Airfoil boundary layer measurements at low Re in an accelerating flow from a nonzero velocity *Exp. Fluids* **11** 368–74
Geyer T F, Claus V T, Hall P M and Sarradj E 2017 Silent owl flight: the effect of the leading edge comb *Int. J. Aeroacoustics* **16** 115–34
Graham R R 1934 The silent flight of owls *Aeronaut. J.* **38** 837–43
Gurka R, Liberzon A and Hetsroni G 2006 POD of vorticity fields: a method for spatial characterization of coherent structures *Int. J. Heat Fluid Flow* **27** 416–23
Gursul I, Vardaki E, Margaris P and Wang Z 2007 Control of wing vortices. Active flow control, notes on numerical fluid mechanics and multidisciplinary design pp 137–51
Hersh A S, Soderman P T and Hayden R E 1974 Investigation of acoustic effects of leading-edge serrations on airfoils *J. Aircr.* **11** 197–202
Hu H, Yang Y, Liu Y, Liu X and Wang Y 2021 Aerodynamic and aeroacoustic investigations of multi-copter rotors with leading edge serrations during forward flight *Aerosp. Sci. Technol.* **112** 106669
Huang H, Dabiri D and Gharib M 1997 On errors of digital particle image velocimetry *Meas. Sci. Technol.* **8** 1427
Ito S 2009 Aerodynamic influence of leading-edge serrations on an airfoil in a low Reynolds number-A study of an owl wing with leading edge serrations *J. Biomech. Sci. Eng.* **4** 117–23
Jaworski J W and Peake N 2020 Aeroacoustics of silent owl flight *Annu. Rev. Fluid Mech.* **52** 395–420
Klaassen van Oorschot B, Tang H K and Tobalske B W 2017 Phylogenetics and ecomorphology of emarginate primary feathers *J. Morphol.* **278** 936–47
Klän S, Bachmann T and Klaas M 2009 Experimental analysis of the flow field over a novel owl-based airfoil *Exp. Fluids* **46** 975–89
Klän S, Burgmann S, Bachmann T, Klaas M, Wagner H and Schröder W 2012 Surface structure and dimensional effects on the aerodynamics of an owl-based wing model *Eur. J. Mech.* B **33** 58–73
Klän S, Klaas M and Schröder W 2010 The influence of leading-edge serrations on the flow field of an artificial owl wing *28th AIAA Applied Aerodynamics Conf.* (*Chicago, Illinois*)
Krishnan K, Ben-Gida H, Morgan G, Kopp G A, Guglielmo C G and Gurka R 2020 Turbulent wake-flow characteristics in the near wake of freely flying raptors: a comparative analysis between an owl and a hawk *Integr. Comp. Biol.* **60** 1109–22
Kroeger R A, Grushka H D and Helvey T C 1972 *Low Speed Aerodynamics for Ultra-quiet Flight* (Tennessee University Space Institute Tullahoma)
Lawley J, Ben-Gida H, Krishnamoorthy K, Hackett E E, Kopp G A, Morgan G, Guglielmo C G and Gurka R 2019 Flow features of the near wake of the Australian boobook owl (*Ninox boobook*) during flapping flight suggest an aerodynamic mechanism of sound suppression for stealthy flight *Integr. Org. Biol.* **1** 1–19
Lee S, Kim J, Park H, Jabłoński P G and Choi H 2015 The function of the alula in avian flight *Sci. Rep.* **5** 9914
Lian Y and Shyy W 2007 Laminar-turbulent transition of a low Reynolds number rigid or flexible airfoil *AIAA J.* **45** 1501–13
Liechti F, Witvliet W, Weber R and Bächler E 2013 First evidence of a 200-day non-stop flight in a bird *Nat. Commun.* **4** 1–7
Lilley G M 1998 A study of the silent flight of the owl *4th AIAA/CEAS Aeroacoustics Conf. Paper* p 2340
Linehan T and Mohseni K 2020 Scaling trends of bird's alular feathers in connection to leading-edge vortex flow over hand-wing *Sci. Rep.* **10** 7905
Lowson M V and Riley A J 1995 Vortex breakdown control by delta wing geometry *J. Aircr.* **32** 832–8
Nafi A, Ben-Gida H, Guglielmo C G and Gurka R 2020 Aerodynamic forces acting on birds during flight: a comparative study of a shorebird, songbird and a strigiform *Exp. Therm. Fluid Sci.* **113** 110018
Narayanan S, Chaitanya P, Haeri S, Joseph P, Kim J W and Polacsek C 2015 Airfoil noise reductions through leading edge serrations *Phys. Fluids* **27** 025109
Neuhaus W, Bretting H and Schweizer B 1973 Morphologische und funktionelle untersuchungen über den lautlosen flug der Eulen (*Strix aluco*) im vergleich zum flug der Enten (*Anas platyrhynchos*) *Biol. Z.* **92** 495–512
Raffel M, Willert C, Wereley S T and Kompenhans J 2007 *Particle Image Velocimetry: A Practical Guide* (Springer)

Rao C, Ikeda T, Nakata T and Liu H 2017 Owl-inspired leading-edge serrations play a crucial role in aerodynamic force production and sound suppression *Bioinsp. Biomim.* **12** 046008

Sarradj E, Fritzsche C and Geyer T 2011 Silent owl flight: bird flyover noise measurements *AIAA J.* **49** 769–79

Schlichting H and Kestin J 2017 *Boundary Layer Theory* 9th edn (McGraw-Hill)

Schwind R G and Allen H J 1973 The effects of leading-edge serrations on reducing flow unsteadiness about airfoils *11th Aerospace Sciences Meeting* pp 73–89

Sturm H, Dumstorff G, Busche P, Westermann D and Lang W 2012 Boundary layer separation and reattachment detection on airfoils by thermal flow sensors *Sensors* **12** 14292–306

Taylor Z J, Kopp G A and Gurka R 2013 Distribution of spanwise enstrophy in the near wake of three symmetric elongated bluff bodies at high Reynolds number *Phys. Fluids* **25** 055103

Wagner H, Weger M, Klaas M and Schröder W 2017 Features of owl wings that promote silent flight *Interface Focus* **7** 20160078

Weger M and Wagner H 2016 Morphological variations of leading-edge serrations in owls (Strigiformes) *PLoS One* **11** e0149236

Winslow J, Otsuka H, Govindarajan B and Chopra I 2018 Basic understanding of airfoil characteristics at low Reynolds numbers *J. Aircr.* **55** 1050–61

Winzen A, Klaas M and Schröder W 2013 High-speed PIV measurements of the near-wall flow field over hairy surfaces *Exp. Fluids* **54** 1472

Winzen A, Klän S, Klaas M and Schröder W 2012a Flow field analysis and contour detection of a natural owl wing using PIV measurements *Nature-Inspired Fluid Mechanics* (Springer) pp 119–34

Winzen A, Klän S, Klaas M, Wagner H and Schröder W 2012b High-speed PIV measurements of the influence of artificial surface structures on the near-wall flow field of 3D wing models based on an owl geometry *16th Int. Symp. on Applications of Laser Techniques to Fluid Mechanics* (*Lisbon, Portugal*)

Winzen A, Roidl B, Klän S, Klaas M and Schröder W 2014 Particle image velocimetry and force measurements of leading-edge serrations on owl-based wing models *J. Bionic Eng.* **11** 423–38

Winzen A, Roidl B and Schröder W 2015 Particle-image velocimetry investigation of the fluid-structure interaction mechanisms of a natural owl wing *Bioinsp. Biomim.* **10** 1–22

Winzen A, Roidl B and Schröder W 2016 Combined particle-image velocimetry and force analysis of the three-dimensional fluid-structure interaction of a natural owl wing *Bioinsp. Biomim.* **11** 026005

Withers P C 1981 An aerodynamic analysis of bird wings as fixed airfoils *J. Exp. Biol.* **90** 143–62